Scripta Materialia 233 (2023) 115513

Contents lists available at ScienceDirect

Scripta Materialia

journal homepage: www.journals.elsevier.com/scripta-materialia

Why rolled Mg-Al-Ca-Mn alloys are less responsive to aging as compared to the extruded

J.J. Bhattacharyya [a,*], T.T. Sasaki [b], T. Nakata [c], S.R. Agnew [a]

[a] University of Virginia, Charlottesville, VA, United States of America
[b] National Institute for Materials Science, Tsukuba, Japan
[c] Nagaoka University of Technology, Nagaoka, Japan

ARTICLE INFO

Keywords:
Texture
Age-hardening
Crystal plasticity
GP zone

ABSTRACT

Dilute Mg-Al-Ca-Mn alloys exhibit excellent strength-ductility combinations in the peak-aged condition due to ordered, single atomic layer Guinier-Preston (GP) zones. The present work explains why rolled sheet material is softer and less responsive to aging, as compared to extruded. Using crystal-plasticity modeling, it is shown that the initial texture of the rolled material permits the soft modes, basal slip and twinning, to accommodate more of the strain during in-plane tension, and they are less responsive to hardening by the finely dispersed GP zones. Even with the same number density of GP zones, the extruded material is stronger in tension along the extrusion axis due to an initial texture which forces higher relative activity of prismatic slip, a mode previously shown to be strongly affected by the GP zones. The present work reemphasizes the significant role of the initial texture in determining the strength and anisotropy of non-cubic metals and alloys.

Age-hardenable Mg alloys based upon dilute additions of Ca together with Al and/or Zn have been developed which exhibit excellent extrudability along with a good balance between high strength and ductility. These dilute Mg alloys are strengthened by a high number density of disk-shaped GP zones lying parallel to the basal plane [1,2]. A recent study has determined the distinct strengthening effect these GP zones have on the various slip and twinning modes in a particular microalloyed, precipitation hardenable Mg alloy, AXM10304 (Mg–1.31Al–0.33Ca–0.46Mn, in wt.%) [3]. It was shown that the basal slip and the extension twinning modes are only modestly strengthened by the GP zones, as compared to the prismatic slip.

Often rolled sheet products are desirable, e.g., for automotive body panels, and thus attempts have been made to develop sheet alloys from the Mg-Al-(Zn)-Ca-Mn system. When the properties of rolled sheets of these Mg-Al-(Zn)-Ca-Mn alloys are compared to the extruded counterparts [2,4-19], it is found that the rolled products have a lower strength compared to the latter (Fig. 1). For instance, both rolled Mg–1.3Al–0.8Zn–0.7Mn–0.5Ca sheet, which exhibits good bake hardenability [14], and rolled Mg–1.1Al–0.3Ca–0.2Mn–0.3 Zn sheet, which shows high Index Erichsen values [12], have lower strengths than the extruded version. One sheet alloy amidst this class of age-hardenable, "lean" Mg alloys, ZAXEM11100 [15] has an exception aging response. However, it is not specifically relevant to the present study because it does not show the high-speed extrudability which is a hallmark of many of the other alloys [20]. This raises the question why the rolled Mg-Al-(Zn)-Ca-Mn alloys are less responsive to aging as compared to the extruded material. The objective of the present work is to provide an answer to this question. The hypothesis is that distinctions in the initial textures of the extruded and rolled materials is responsible, and a polycrystal plasticity-based approach is employed to test this hypothesis.

Mg-1.2Al-0.4Ca-0.5Mn (wt.%) alloy sheets with 260 mm width and 4 mm thickness were prepared by the twin-roll casting (TRC) process. The TRC sheets were first homogenized in a muffle furnace at 450 °C for 2 h, followed by water quenching. The homogenized sheets were then rolled to obtain 1 mm thick plates with ~30% thickness reduction per pass. Between each rolling pass, the sheets were reheated at 450 °C for 5 min. The as-rolled sheets were then solution treated at 450 °C for 1 h in a muffle furnace and quenched into water. A part of the specimens was artificially aged to the peak hardness, i.e., 170 °C for 2 h in an oil bath. Details of the age hardening behavior of alloys from this system are presented elsewhere [2,4-6,9]. Tensile test specimens with gage length and width of 12.5 and 5 mm were machined from the solution-treated and peak-aged samples. Electron backscatter diffraction (EBSD)

* Corresponding author.
E-mail address: jjb4cp@virginia.edu (J.J. Bhattacharyya).

https://doi.org/10.1016/j.scriptamat.2023.115513
Received 6 March 2023; Received in revised form 13 April 2023; Accepted 22 April 2023
Available online 26 April 2023

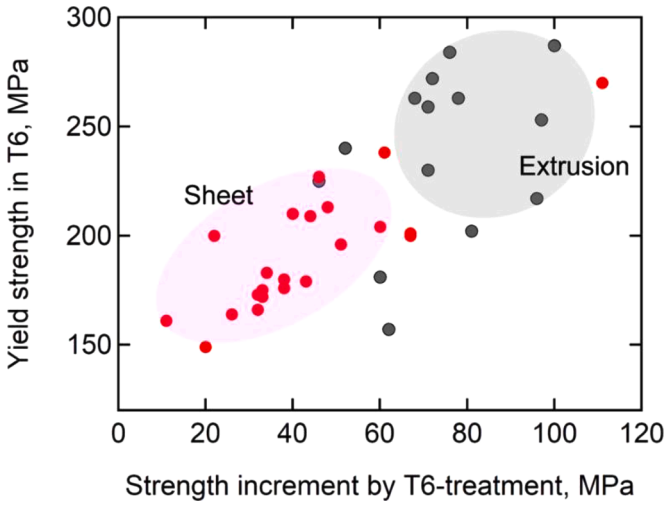

Fig. 1. A plot of the yield strength as a function of strength increment during aging, showing the relative age-hardenability of various "lean" Mg alloys reported in the literature [2,4–19] emphasizing that extruded alloys are more responsive than rolled.

analysis was performed using a field emission scanning electron microscope (FE-SEM), Carl Zeiss Cross Beam 1540EsB, equipped with an Oxford Instruments HKL Channel 5 electron EBSD system. Specimens for the EBSD analysis were prepared by mechanical polishing. The experimental twin volume fraction is obtained from the EBSD data, using the MTEX (version 5.8.1) toolbox [21]. In brief, the $\{\bar{1}012\}$ extension twin boundaries are identified based on the misorientation relation $86.3^\circ\langle\bar{1}210\rangle$ with a 5° tolerance. Next, the parent grains are reconstructed using the MTEX function *merge* where all grains that have a common twinning boundary are merged. By assuming that the twins consume less than half of the parent grain, an assumption which is fitting in the present study due to the strain paths and levels of strain explored, the volume fraction is obtained as $\frac{Area_{twinned}}{total\ grain\ area}$. For further details the reader is referred to [22]. Transmission electron microscopy (TEM) and atom probe tomography (APT) analyses were carried out using an FEI Titan G2 80–200 TEM operating at 200 kV and a local electrode atom probe (CAMECA LEAP 5000 XS) in voltage pulse mode at a temperature of 30 K, respectively. Thin foil specimens for TEM analysis were prepared using the precision ion mill (JEOL EM-09100IS Ion Slicer). Needle-shaped specimens for the APT were prepared using the focused ion beam (FIB) lift-out and annular milling techniques with an FEI Helios G4 UX.

Fig. 2a shows the initial texture of rolled AXM100. The hot rolling process results in a relatively weak texture with a maximum intensity of 3.2 multiples of a random distribution (m.r.d) in the (0002) pole figure, with the highest intensity position tilted by 15–30° towards the rolling direction (RD). Notably, there is also significant spread of the basal poles along the transverse direction (TD). The $(10\bar{1}0)$ pole figure shows only a slight preference for alignment of the prismatic poles with the RD. The EBSD normal direction (ND) inverse pole figure (IPF) map shows an equiaxed, uniform grain structure with an average grain size of 8.0 μm (Fig. 2b), which is quite similar[1] to the grain size of the extruded [2,3] and rolled products of the same alloy [12].

Fig. 2c and d show the bright-field (BF) TEM micrograph and 3D atom map of the peak-aged sample, respectively. The BF-TEM image was taken from the zone axis of $[01\bar{1}0]$, and Fig. 2c includes the selected area electron diffraction (SAED) pattern in the inset. The GP zones are densely dispersed on the (0002) planes of the matrix, as is clear from the strain contrast in the BF-TEM micrograph and the continuous streaks along the [0001] direction of the Mg matrix at the $1/3\{11\bar{2}0\}$ and $2/3\{11\bar{2}0\}$ positions, as shown in the SAED pattern. The 3D atom map in Fig. 2d shows that the enrichment of Ca and Al within the GP zones, and the number density of the GP zones is $\sim 9.6 \times 10^{23}\ m^{-3}$. These microstructural features are close to that of the peak aged microstructure of Mg-1.31Al-0.33Ca-0.46Mn (wt.%) alloy extrusions reported previously, despite the slight differences in the composition (within ~0.1 wt.% for each element) of the two alloys [2,3].

Fig. 3a and b show the tensile stress-strain curves along RD and TD of the solutionized and peak-aged alloy sheets. The solutionized material has a yield strength of 160 MPa along RD and 130 MPa along TD. The peak-aging (T6) treatment (170 °C, 2 h) increases the yield strength to 220 and 180 MPa, for RD and TD respectively. This implies an increase of ~ 50 MPa which is associated with the dense dispersion of the aforementioned Al/Ca-rich GP zones on the basal planes of the Mg matrix [2,3]. For ease of comparison, Figs. 3c and d show previously published stress-strain curves for tension and compression along the extrusion direction (EDt and EDc respectively) as well as compression along the radial direction (RaDc) for the extruded material. ED tension shows the largest increase in yield strength (~180 to ~300 MPa) followed by RaDc (~90 to ~140 MPa) and EDc (~150 to ~180 MPa). Based on this data from extruded material, a set of strength and hardening parameters for a crystal plasticity model was developed in our previous work [3], and it was shown that the prismatic slip is most strongly affected by the GP zones, whereas only a marginal strengthening effect is observed by the basal slip and the twinning modes. In the present work, the Elasto-ViscoPlastic Self-Consistent (EVPSC) code is used and the same model parameters which were used to describe the extruded material, were used to predict the response of the rolled material, in both solutionized and peak-aged condition (Table 1).

The simulated curves shown in Fig. 3 reveal that the yield behavior of the rolled material is accurately predicted using the same strength parameters that were developed for the extruded material. Notably the lower strength as compared to the extruded, as well as the yield anisotropy between RD and TD is accurately described, for both the solutionized and the peak-aged material.

Note that the grain sizes and the solute contents of the solutionized materials of the two product forms are very similar. Furthermore, the size and number density of the GP zones in the peak aged rolled and extruded materials are almost identical. The agreement between predictions of the single polycrystal model and the experimentally observed behaviors of both product forms suggests that the model indeed accurately accounts for the Hall-Petch grain size effects, solute strengthening, and even the strengthening effect of the shearable GP zones on each individual deformation mode, regardless of straining direction and product form.

The model also predicts relative activities of the deformation modes for the solutionized and peak-aged extruded and sheet material (Fig. 4a and b). For ED tension, the initial texture is such that the prismatic slip is favored throughout, accompanied by some twinning activity at low strains. On the other hand, the rolled texture is such that basal slip accommodates a large fraction of the strain. Only at later stages does the prismatic slip dominate in case of in-plane tension. The twinning activities increase slightly after aging, whereas the activities of the other deformation modes remain qualitatively similar to the solutionized case (Fig. 4b). The measured and simulated twin volume fraction for the sheet material (Fig. 4c) confirms the larger twin activity for the predicted for the TD tension case, relative to the RD (Fig. 4a and b). This latter result is due to the spread of the basal poles towards TD in the initial texture of the rolled sheet. Finally, this leads to a slightly higher level of twinning activity and slightly softer response as compared to RD.

It is worth mentioning that the apparent overestimation of the

[1] In the previous study a mean grain size of 15 μm was reported, which was obtained by considering grains larger than 5 μm. If all the grains are considered, a mean grain size of 7 μm is obtained.

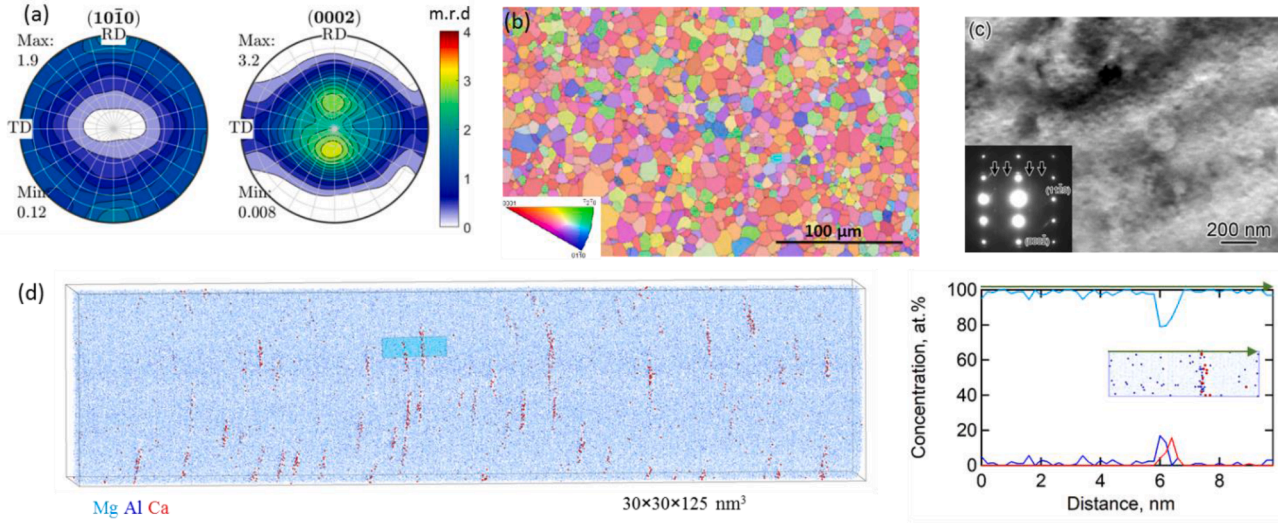

Fig. 2. Initial texture and microstructure of rolled AXM100 sheet (a) (10$\bar{1}$0) and (0002) pole figures of the T4 treated material (b) EBSD ND-IPF map of T6 material showing equiaxed grain structure (c) a bright-field TEM micrograph taken along the [01$\bar{1}$0] zone axis, from the T6 material. The selected area electron diffraction (SAED) pattern shows continuous streaks along the [0001] direction of the Mg matrix. (d) the 3D atom map from the same material shows enrichment of Ca and Al within the GP zones and a number density of $\sim 9.6 \times 10^{23}\ m^{-3}$.

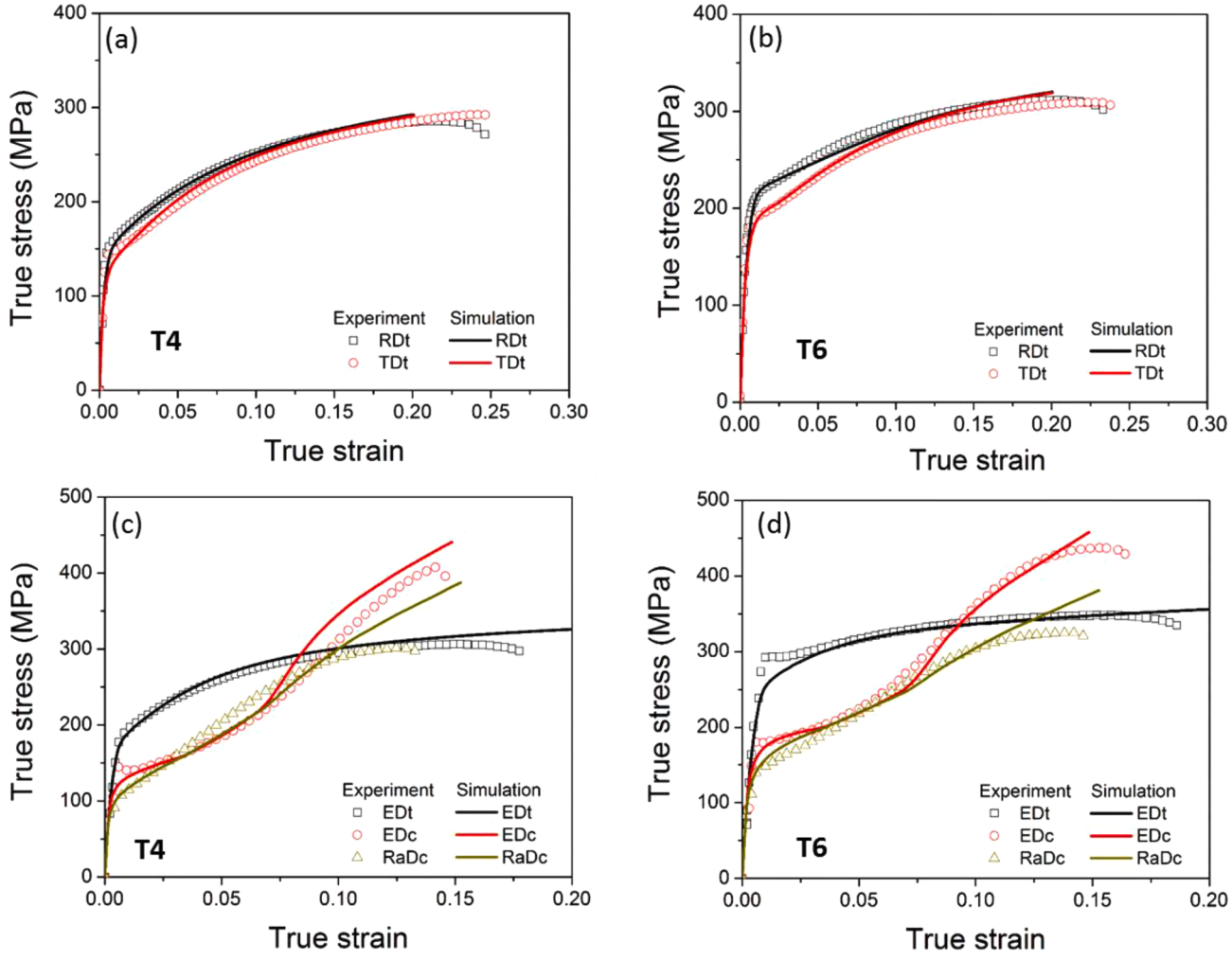

Fig. 3. Experimental and simulated stress-strain curves for tension along RD and TD, for the rolled AXM100 sheet in (a) T4 condition and (b) T6 condition. ED tension and compression and radial direction compression (RaDc) data for the extruded material in (c) T4 condition and (d) in T6 condition. Based on this data from the extruded material, a crystal plasticity model was developed which is used to predict the response of the rolled sheet.

Table 1
The Voce hardening parameters developed for the T4 temper and the T6 temper of the extruded material [3]. By using the same initial CRSS $\tau_{i,0}$, the response of the rolled material was predicted. The hardening parameters $\tau_{i,1}$ and $\theta_{i,0}$were adjusted to match the experimental strain hardening behavior of the rolled material.

Deformation mode	$\tau_{i,0}$		$\tau_{i,1}$		$\theta_{i,0}$	
	T4	T6	T4	T6	T4	T6
Basal	20	30	55	1	100	100
Prismatic	101	140	20	1	100	100
$<c+a>$	140	180	250	250	500	500
TTW	46	61	0	0	1	1

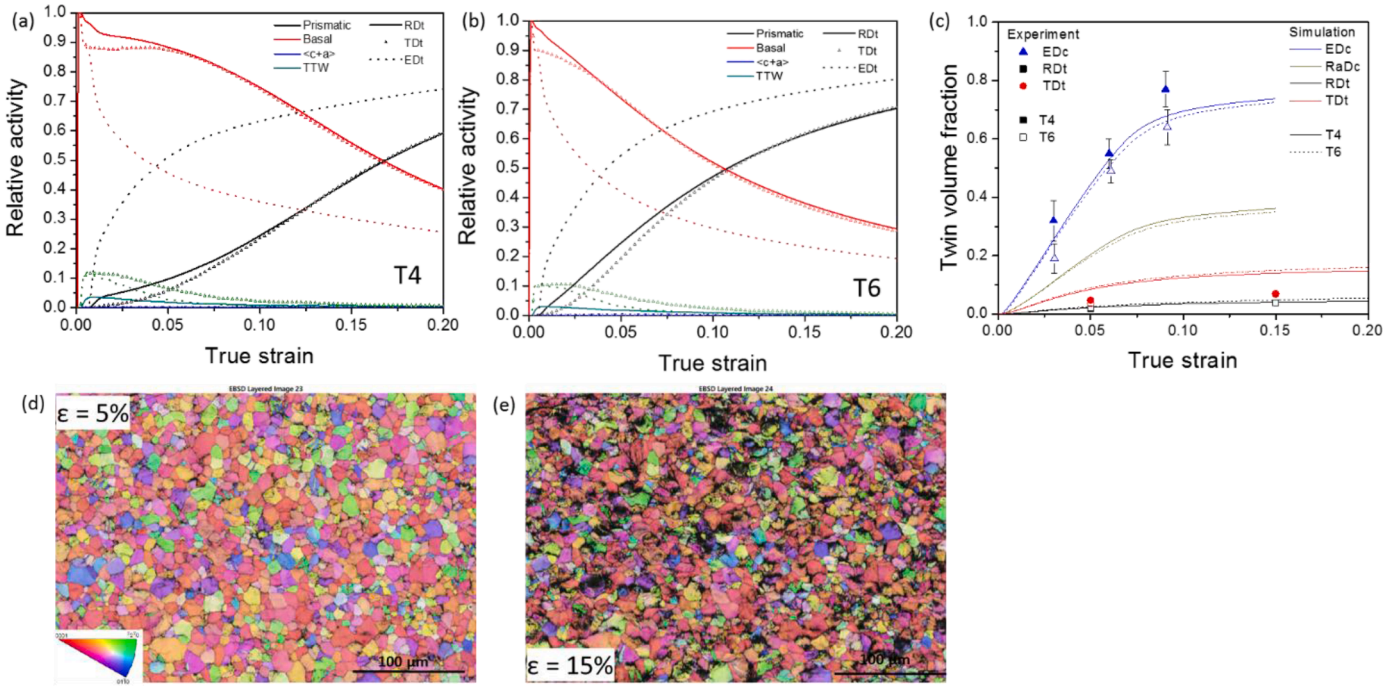

Fig. 4. Relative activity of deformation modes obtained from the EVPSC simulations of the rolled sheet tested in tension along RD (solid lines) and TD (symbol) for (a) T4 and (b) T6 material. Relative activities for ED tension of the extruded material is also shown using dotted lines for comparison. (c) Evolution of the twin volume fraction (experimental and simulated) for RD and TD tension of the sheet material as well as the twin dominated cases of ED and radial direction compression (RaDc) of the extruded material are shown. EBSD ND-IPF map of the T6 material tested in tension along TD after (d) 5% strain and (e) 15% strain, showing a decrease in the fraction of indexed points with straining. The unstrained map is shown in Fig. 2b.

simulated twin volume fraction for the in-plane tension case, especially at larger strains, is most likely due to the degradation of the EBSD diffraction patterns at larger strains, which leads to a decrease in the fraction of indexed points, e.g. for the T6 material, fraction of indexed points ~95% before straining (Fig. 2b), which degrades to ~90% after strain of 0.05 (Fig. 4d), and to ~70% after strain of 0.15 (Fig. 4e), when tested in tension along TD. Indexing hit rate for all the samples investigated in the present work are listed in Table S1. It has been shown that these non-indexed points are frequently associated with twins [23]. The grain boundary misorientation axis and angle distribution (Fig. S1) also shows the presence of a large fraction of the twin boundaries 86.3 $^{\circ}\langle\bar{1}210\rangle$ after 15% strain for the peak-aged RDt and TDt. The twin boundary fraction is slightly larger in case of TDt as compared to RDt, again confirming that the TD oriented sample is more prone to twinning by virtue of the initial texture.

In relationship to previous studies of extruded material, the relative activity plots presented in Fig. 4 explain why in-plane tension of the rolled sheet is softer than EDt; the latter is controlled by prismatic slip and shows the largest strength increment after age-hardening. Readers are reminded that the twinning-controlled EDc (Fig. S2) shows only a modest strength increase upon aging, which helps explain why there is an increased level of twinning in the sheet material after aging since its strength *relative to the other modes* actually drops. Finally, basal slip-controlled RaDc (Fig. S2) shows a strength increment which lies between EDt and EDc. For the purpose of comparison, Fig. 4b reiterates the twin volume fraction evolution for the EDc and RaDc cases [3]. These two loading conditions are such that twinning accommodates a large amount of strain and thus a significant portion of the matrix is twinned after 15% strain.

It is worth mentioning that the hardening parameters had to be adjusted in order to match the strain hardening behavior of the rolled sheet. The strain hardening of the basal slip and twinning modes had to be reduced, and it was found that almost no mode-level hardening is required to match the experimental curves.[2] This result of low strain hardening for basal slip is in keeping with the early single crystal strain hardening study of Hirsch and Lally [24]. This also suggests that the hardening exhibited by the experimental, polycrystalline flow curves mainly arises from intergranular interactions and so-called "geometric hardening" due to texture evolution [25]. Figs. S3 and S4 show the experimental and simulated texture of the rolled sheet after deformation. After 15% strain (Fig. S3), clear evidence of prismatic slip-induced

[2] *Note in-plane compression data is required to identify accurately the twin hardening parameters. Similarly, ND compression data is required to determine both the strength and the hardening parameters of the $<c+a>$ slip.*

texture evolution is observed, where the prismatic poles align with the straining direction (RD or TD) and the basal poles spread along TD and RD for RDt and TDt respectively. Note, the grains that are initially favorably oriented for twinning (i.e. c-axis initially aligned with the straining direction) reorient such that the c-axes of the twins align near to the ND. This is a hard orientation which subsequently accommodates strain by prismatic slip. This texture evolution is responsible for the strain hardening that is observed in the experiments and simulations. Since a lower fraction of grains are favorably oriented for twinning in case of ED tension, this texture hardening contribution is small and thus the experimental flow curve shows a lower hardening rate as compared to in-plane tension of the rolled sheet. Note, for both the extruded and the rolled material, no hardening of the prismatic slip is required (i.e. τ_1 is set to 1). The results suggest that a dislocation-density based strain hardening rule in which the basal slip model is potently affected by the activity of other (e.g., prismatic) slip systems merits further exploration. A first exploration of this issue is represented by the discrete dislocation dynamics study of Bertin and Capolungo [26].

In conclusion, it is shown that a single polycrystal plasticity-based model of alloy strength can accurately predict the behavior of new, dilute Mg alloys with Ca along with Al and/or Zn regardless of product form. The results provide a satisfying (self-consistent) explanation for why the tensile yield strengths of rolled sheets are lower and why they exhibit a lower age-hardening response, as compared to extruded bars. As a corollary, the sheet material benefits from greater geometric (texture evolution-induced) strain hardening, which results in higher elongations than those exhibited by the extruded material.

Declaration of Competing Interest

The authors declare that they have no known competing financial interests or personal relationships that could have appeared to influence the work reported in this paper.

Acknowledgments

This work is supported by the U.S. National Science Foundation (NSF) DMREF grant CMMI-1921926. T.T. Sasaki acknowledges the support by JSPS KAKENHI (Grant Number JP21H01675) and The Light Metal Educational Foundation, Inc., Japan.

Supplementary materials

Supplementary material associated with this article can be found, in the online version, at doi:10.1016/j.scriptamat.2023.115513.

References

[1] K. Hono, C.L. Mendis, T.T. Sasaki, K. Oh-Ishi, Towards the development of heat-treatable high-strength wrought Mg alloys, Scr. Mater. 63 (2010) 710–715, https://doi.org/10.1016/j.scriptamat.2010.01.038.

[2] T. Nakata, C. Xu, R. Ajima, K. Shimizu, S. Hanaki, T.T. Sasaki, L. Ma, K. Hono, S. Kamado, Strong and ductile age-hardening Mg-Al-Ca-Mn alloy that can be extruded as fast as aluminum alloys, Acta Mater. 130 (2017) 261–270, https://doi.org/10.1016/j.actamat.2017.03.046.

[3] J.J. Bhattacharyya, T. Sasaki, T. Nakata, K. Hono, S. Kamado, S.R. Agnew, Determining the strength of GP zones both parallel and perpendicular to the zone, Acta Mater. 171 (2019) 231–239.

[4] T. Nakata, C. Xu, T.T. Sasaki, Y. Matsumoto, K. Shimizu, K. Hono, S. Kamado, Development of High-Strength High-Speed-Extrudable Mg–Al–Ca–Mn Alloy, in: K. N. Solanki, D. Orlov, A. Singh, N.R. Neelameggham (Eds.), Magnes. Technol. 2017, Springer International Publishing, Cham, 2017, pp. 17–21.

[5] T. Nakata, C. Xu, R. Ajima, Y. Matsumoto, K. Shimizu, T.T. Sasaki, K. Hono, S. Kamado, Improving mechanical properties and yield asymmetry in high-speed extrudable Mg-1.1Al-0.24Ca (wt%) alloy by high Mn addition, Mater. Sci. Eng. A. 712 (2018) 12–19, https://doi.org/10.1016/j.msea.2017.11.085.

[6] M. Cihova, R. Schäublin, L.B. Hauser, S.S.A. Gerstl, C. Simson, P.J. Uggowitzer, J. F. Löffler, Rational design of a lean magnesium-based alloy with high age-hardening response, Acta Mater. 158 (2018) 214–229, https://doi.org/10.1016/j.actamat.2018.07.054.

[7] X. Liu, X. Qiao, Z. Li, M. Zheng, High strength and excellent ductility of dilute Mg-0.68Al-0.32Ca-0.50Mn (wt%) extrusion alloy obtained by T6 treatment, Mater. Charact. 162 (2020), 110197, https://doi.org/10.1016/j.matchar.2020.110197.

[8] Z.-.M. Hua, C. Wang, T.-.S. Wang, C. Du, S.-.B. Jin, G. Sha, Y. Gao, H.-.L. Jia, M. Zha, H.-.Y. Wang, Large hardening response mediated by room-temperature dynamic solute clustering behavior in a dilute Mg-Zn-Ca-Sn-Mn alloy, Acta Mater. 240 (2022), 118308, https://doi.org/10.1016/j.actamat.2022.118308.

[9] J. Zuo, T. Nakata, C. Xu, Y.P. Xia, H.L. Shi, G.S. Wang, G.Z. Tang, G.H. Fan, S. Kamado, L. Geng, Effect of annealing on microstructure evolution and age-hardening behavior of dilute Mg–Al–Ca–Mn alloy, J. Mater. Res. Technol. 18 (2022) 1754–1762, https://doi.org/10.1016/j.jmrt.2022.03.091.

[10] Z.R. Zeng, Y.M. Zhu, M.Z. Bian, S.W. Xu, C.H.J. Davies, N. Birbilis, J.F. Nie, Annealing strengthening in a dilute Mg–Zn–Ca sheet alloy, Scr. Mater. 107 (2015) 127–130, https://doi.org/10.1016/j.scriptamat.2015.06.002.

[11] M.Z. Bian, Z.R. Zeng, S.W. Xu, S.M. Zhu, Y.M. Zhu, C.H.J. Davies, N. Birbilis, J. F. Nie, Improving Formability of Mg–Ca–Zr Sheet Alloy by Microalloying of Zn, Adv. Eng. Mater. 18 (2016) 1763–1769, https://doi.org/10.1002/adem.201600293.

[12] M.Z. Bian, T.T. Sasaki, B.C. Suh, T. Nakata, S. Kamado, K. Hono, A heat-treatable Mg–Al–Ca–Mn–Zn sheet alloy with good room temperature formability, Scr. Mater. 138 (2017) 151–155, https://doi.org/10.1016/j.scriptamat.2017.05.034.

[13] M.Z. Bian, T.T. Sasaki, B.C. Suh, T. Nakata, S. Kamado, K. Hono, Development of Heat-Treatable High-Strength Mg–Zn–Ca–Zr Sheet Alloy with Excellent Room Temperature Formability, in: D. Orlov, V. Joshi, K.N. Solanki, N.R. Neelameggham (Eds.), Magnes. Technol. 2018, Springer International Publishing, Cham, 2018, pp. 361–364.

[14] M.Z. Bian, T.T. Sasaki, T. Nakata, Y. Yoshida, N. Kawabe, S. Kamado, K. Hono, Bake-hardenable Mg–Al–Zn–Mn–Ca sheet alloy processed by twin-roll casting, Acta Mater. 158 (2018) 278–288, https://doi.org/10.1016/j.actamat.2018.07.057.

[15] R. Shi, J. Miao, T. Avey, A.A. Luo, A new magnesium sheet alloy with high tensile properties and room-temperature formability, Sci. Rep. 10 (2020) 18–23, https://doi.org/10.1038/s41598-020-67161-9.

[16] Z.H. Li, T.T. Sasaki, T. Shiroyama, A. Miura, K. Uchida, K. Hono, Simultaneous achievement of high thermal conductivity, high strength and formability in Mg-Zn-Ca-Zr sheet alloy, Mater. Res. Lett. 8 (2020) 335–340, https://doi.org/10.1080/21663831.2020.1759718.

[17] Z.H. Li, T.T. Sasaki, M.Z. Bian, T. Nakata, Y. Yoshida, N. Kawabe, S. Kamado, K. Hono, Role of Zn on the room temperature formability and strength in Mg–Al–Ca–Mn sheet alloys, J. Alloys Compd. 847 (2020) 1–11, https://doi.org/10.1016/j.jallcom.2020.156347.

[18] Y.-.J. Li, Y. Fang, C. Wang, Z.-.M. Hua, Y. Gao, M. Zha, H.-.Y. Wang, Enhanced strength-ductility synergy achieved through twin boundary pinning in a bake-hardened Mg–2Zn-0.5Ca alloy, Mater. Sci. Eng. A. 831 (2022), 142239, https://doi.org/10.1016/j.msea.2021.142239.

[19] S. Jo, J. Bohlen, G. Kurz, Individual contribution of Zn and Ca on age-hardenability and formability of Zn-based magnesium alloy sheet, Mater. (Basel) 15 (2022), https://doi.org/10.3390/ma15155239.

[20] T. Avey, J. Miao, J. Caris, A.K. Sachdev, A. Luo, Processing map and performance of a low-cost wrought magnesium alloy: ZAXEM11100, in: S. Barela, A. Leonard, P. Maier, N.R. Neelameggham, V.M. Miller (Eds.), Magnes. Technol. 2023, Springer Nature Switzerland, Cham, 2023, pp. 189–195.

[21] F. Bachmann, R. Hielscher, H. Schaeben, Grain detection from 2d and 3d EBSD data-specification of the MTEX algorithm, Ultramicroscopy 111 (2011) 1720–1733, https://doi.org/10.1016/j.ultramic.2011.08.002.

[22] D.J. Savage, R.J. McCabe, M. Knezevic, An automated procedure built on MTEX for reconstructing deformation twin hierarchies from electron backscattered diffraction datasets of heavily twinned microstructures, Mater. Charact. (2021) 171, https://doi.org/10.1016/j.matchar.2020.110808.

[23] M.R. Barnett, M.D. Nave, C.J. Bettles, Deformation microstructures and textures of some cold rolled Mg alloys, Mater. Sci. Eng. A. 386 (2004) 205–211, https://doi.org/10.1016/j.msea.2004.07.030.

[24] P.B. Hirsch, J.S. Lally, The deformation of magnesium single crystals, Philos. Mag. 12 (1965) 595–648.

[25] C. Tome, G.R. Canova, U.F. Kocks, N. Christodoulou, J.J. Jonas, The relation between macroscopic and microscopic strain hardening in f.c.c. polycrystals, Acta Met. 32 (1984) 1637–1653.

[26] N. Bertin, C.N. Tomé, I.J. Beyerlein, M.R. Barnett, L. Capolungo, On the strength of dislocation interactions and their effect on latent hardening in pure Magnesium, Int. J. Plast. 62 (2014) 72–92, https://doi.org/10.1016/j.ijplas.2014.06.010.